Applied Surface Science 333 (2015) 78–85

Contents lists available at ScienceDirect

Applied Surface Science

journal homepage: www.elsevier.com/locate/apsusc

MnO_2/Au hybrid nanowall film for high-performance surface-enhanced Raman scattering substrate

Minghui Zhou [a], Xiaoli Liu [b], Baozhi Yu [a], Jing Cai [b], Chunyan Liao [a], Zhenhua Ni [c], Zhongyue Zhang [d], Zhaoyu Ren [a], Jintao Bai [a], Haiming Fan [a,b,*]

[a] Institute of Photonics & Photon-Technology, Northwest University, Xi'an 710069, China
[b] School of Chemical Engineering, Northwest University, Xi'an 710069, China
[c] Department of Physics, Southeast University, Nanjing 211189, China
[d] College of Physics and Information Technology, Shaanxi Normal University, Xi'an 710062, China

ARTICLE INFO

Article history:
Received 15 November 2014
Received in revised form 16 January 2015
Accepted 2 February 2015
Available online 11 February 2015

Keywords:
MnO_2/Au nanowall film
Surface-enhanced Raman Scattering (SERS) substrate
Raman mapping

ABSTRACT

Surface-enhanced Raman scattering (SERS) technology has been investigated for long time because of its tremendous potential in chemical and biomolecular detection. One of the challenging works in this field is to fabricate fantastic substrates with high sensitivity, stability, and reproducibility. This work reports a novel SERS substrate based on MnO_2/Au hybrid nanowall film prepared by simple and cheap hydrothermal method combined with subsequent vacuum thermal evaporation process. Enhanced SERS enhancement factor (EF) with increased thickness of gold layer was observed and a significant increase of EF up to 8 orders of magnitude has been achieved. Finite-difference time-domain (FDTD) simulations have been carried out to elucidate the origin of the enhancement and the distribution of the "hot spots". Experimental evidences indicate that the as-prepared substrate possesses excellent SERS sensitivity, good stability and high reproducibility. Our results provide a novel MnO_2/Au hybrid nanowall film as a convenient and robust SERS-active substrate for detecting biomolecules.

© 2015 Elsevier B.V. All rights reserved.

1. Introduction

Since its discovery in 1974 by Fleischman [1], surface-enhanced Raman scattering (SERS) is recognized as an effective tool with high sensitivity for diverse applications, such as biology, chemistry, environment and archaeology[2]. So far, much effort has been devoted to the investigations of SERS. In particular, due to its non-destructive, narrow signal bandwidth, multiplexing capability and label-feel detectability, SERS recently has been attracted much attention for biomolecule detection, medical diagnosis and high resolution cellular imaging [3,4]. The ability of single-molecule detection makes SERS a more fascinating technology with superhigh sensitivity [5,6]. However, the instability and low reproducibility of detection signal as well as the relatively low sensitivity attributed to inappropriate substrate largely hinder their further practical applications [7,8]. Therefore, the development of novel SERS substrates with high sensitivity, stability, and reproducibility is of utmost importance for practice applications [9].

Currently, noble metal nanostructures are widely investigated in the fabrication of SERS substrate, such as gold nanospheres [10], gold nanoflowers [11], silver nanorods [12], silver nanodendrites [13] and gold/silver multilayered nanostructures [14]. However, the high cost of these nanostructures restricts their application in routine work. Thanks for the rapid development in chemical synthesis, various semiconductor or semiconductor oxide nanostructures now can be prepared with tunable morphologies and band gap by inexpensive and green solution route [15]. In this context, hybrid nanostructures obtained by combining environment-friendly semiconductor with noble metal have shown great potential as SERS substrates because of its large surface area, abundant micro/nano structure and ease to charge transfer between semiconductor and noble metal [16,17]. In comparison with pristine noble metal substrates, semiconductor-noble metal hybrid nanostructures can provide a high density of "hot spots" for localized surface plasmon resonance (LSPR), absorb a large number of probe molecules in finite detection volume, and append additional chemical enhancement [16]. Up to now, many semiconductor-noble metal hybrid nanostructures have been developed as SERS substrates such as ZnO/Ag [17–19], Si/Ag [20–22], TiO_2/Ag [23,24] and MnO_2/Ag (Au) [25,26]. Various hybrid structures include ZnO nanorods coated with Ag [17], porous Si

* Corresponding author. Tel.: +86 29 88302747.
E-mail address: fanhm@nwu.edu.cn (H. Fan).

http://dx.doi.org/10.1016/j.apsusc.2015.02.014
0169-4332/© 2015 Elsevier B.V. All rights reserved.

decorated with Ag [23], Fe_2O_3/Ag core-shell nanostructures [27], carbon nanowalls interspersed with Ag nanoparticles [28] and MnO_2 nanospheres enclosed with Au have been investigated [26]. For example, MnO_2-Ag nanocomposite has been verified a promising choice for SERS substrates and the enhancement factor (EF) up to 10^6 has been achieved [26]. However, the fabrication of robust and large-area substrate is still urgent because the above-mentioned substrates are either core/shell nanoparticles that have to further assemble into active substrate, or the nanowire/nanorod arrays that require complex fabrication process to achieve uniform areal density.

Herein, MnO_2/Au hybrid nanowall film has been fabricated through a simple and cheap hydrothermal treatment, followed by gold coating using vacuum thermal evaporation process. The sensitivity, stability and reproducibility of the obtained substrates have been evaluated by a series of Raman spectroscopy measurement. Especially, Raman mapping are employed to study the reproducibility in a large area. The local electric field enhancement and the "hot spots" distribution of the substrate are also analyzed by finite-difference time-domain (FDTD) simulation. The results obtained from this study not only provide a robust SERS substrate fabricated by cheap and facile approach, but also adopt Raman mapping technique to evaluate the performance of SERS substrate.

2. Experimental

The MnO_2 nanowall film was synthesized by using the hydrothermal method reported previously [29]. In a typical experimental procedure, the silicon wafers were thoroughly cleaned with deionized water in an ultrasound bath for minutes. Afterward gold seeds coating was performed with ion sputtering method on the polished side of silicon wafer. 2.5 mM potassium permanganate ($KMnO_4$) powder and 10 mM concentrated hydrochloric acid were added to 45 mL of deionized water to form a precursor solution, which was then transferred into a Teflon-lined stainless steel autoclave with a capacity of 100 mL. The silicon wafers were leaning on the wall of autoclave with polished side face down. They were used as the supporting materials to grow homogeneous MnO_2 nanowall film. The autoclave was sealed and treated hydrothermally at 140 °C for 50 min to obtain the nanowall film. All the as-prepared films were washed with deionized water several times to remove residual MnO_2 powder or other impurities, and then dried in air.

Gold was then coated on the MnO_2 nanowall film substrates by vacuum thermal evaporation method (Technol ZHD-400, vacuum degree 5×10^{-4} Pa). Substrates with different nominal thickness of gold film were monitored by the film-thickness monitor (Taiyao FTM-V) with a relative average error less than 5%. The deposition rate is about 0.1 Å/s through all the procedure. The obtained hybrid samples are labelled based on different nominal thickness of gold layer, for example, a substrate coated with 20 nm gold is labelled as "Substrate-20". X-ray diffraction (XRD) data were acquired by an X'pert Pro Panalytical X-ray diffractometer (radiation source: Cu K_α, current: 40 mA, voltage: 40 kV). The typical morphologies of MnO_2 nanowall film and MnO_2/Au hybrid nanowall film were characterized by scanning electron microscope (SEM; FEI INSPECT F50) equipped with an Energy-dispersive X-ray spectroscopy (EDS) detector and transmission electron microscope (TEM; FEI Tecnai G2 F20 S-TWIN).

Crystal violet (CV) was purchased from Aladdin Industrial Inc. and was used for Raman measurements without further purification. A series of concentrations (from 10^{-4} to 10^{-10} M) of CV aqueous solutions were prepared. The analyte solutions were dropped onto the substrates and dried in air. Then the substrates were used for Raman measurements directly using a confocal Raman system (WITec alpha 300). All of the spectra were collected in backscattering geometry with a 20 × objective (NA = 0.4), the excitation laser wavelength was 532 nm with a spot diameter ca. 2 μm. A 10 s acquisition time and ca. 215 μW laser power were used to acquire SERS spectra in all single spectrum cases. All of the SERS spectra and maps were analyzed using the WITec Project 2.10 data evaluation software equipped in the Raman system. The Raman band of a silicon wafer at 521 cm^{-1} was employed to calibrate the spectrometer.

3. Results and discussion

Conventional top-down methods such as nanosphere lithography [30], electron beam lithography [31], optical lithography [32] and nanoimprint lithography [33] are high cost and of low feasibility for fabrication of large-area SERS substrates, so that they are not suitable for industrial applications. However, the combination of chemical synthesis with ion sputtering, electroplating or thermal evaporation has attracted extensive attention because of its cheap and convenient fabrication process. Fig. 1 illustrates the experimental schematic of the fabrication and test procedure of

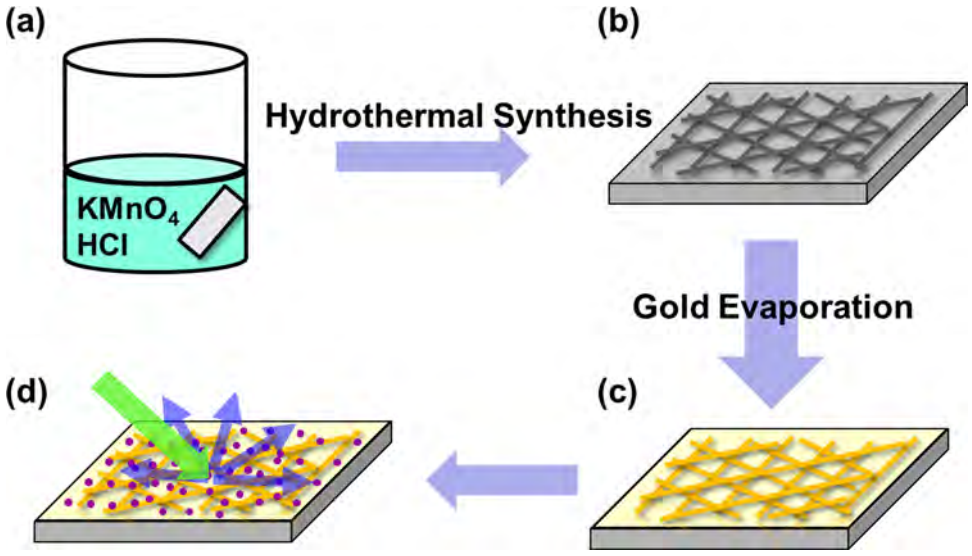

Fig. 1. Schematic illustration of overall experimental process.

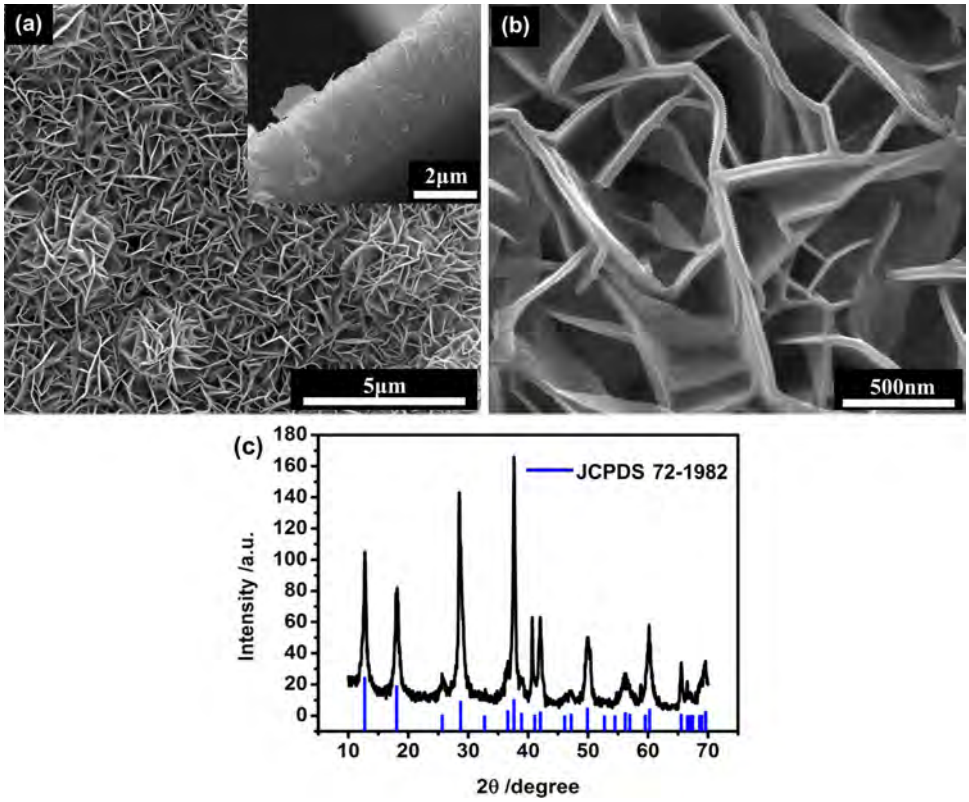

Fig. 2. (a) The top-view SEM image of MnO_2 nanowall film on silicon wafer, the inset is the cross-section view of the MnO_2 nanowall film; (b) the high magnification SEM image of the MnO_2 nanowall film; (c) the XRD pattern of the MnO_2 nanowall film.

the MnO_2/Au hybrid nanowall film. Facile hydrothermal method was adopted for the synthesis of MnO_2 nanowall film (Fig. 1(a)), then a gold evaporation process was carried out to obtain the MnO_2/Au hybrid nanowall film (Fig. 1(b) and (c)). Fig. 2(a) shows the top-view SEM image of as-prepared MnO_2 nanowall film. As shown in Fig. 2(a), nanowalls are inter-connectedly and vertically grown on the silicon wafer surface with uniform density. These nanowalls have a three-dimensional structure with a thickness of ca. 40 nm and a total height of ca. 3 μm as shown in the side-view SEM image (inset of Fig. 2(a)). Fig. 2(b) shows the high magnification SEM image of nanowall film, and a honeycomb structure is formed, which benefits the adsorption of biomolecule to be determined. The crystal phase of MnO_2 nanowall film hydrothermally grown from the silicon wafer is identified by XRD pattern (Fig. 2(c)). The result shows that all diffraction peaks can be exclusively indexed as α-MnO_2 (JCPDS 72-1982), indicating that the MnO_2 nanowalls are well crystallized. After the deposition of 5 nm gold on it, some gold nanoparticles appear on the top and side position of nanowalls as shown in Fig. 3(a). The EDS analysis further verifies the combination of MnO_2 and gold (Fig. S1). With the thickness of gold layer increasing, the density of nanoparticles increases continuously and a rugged gold surface with dense

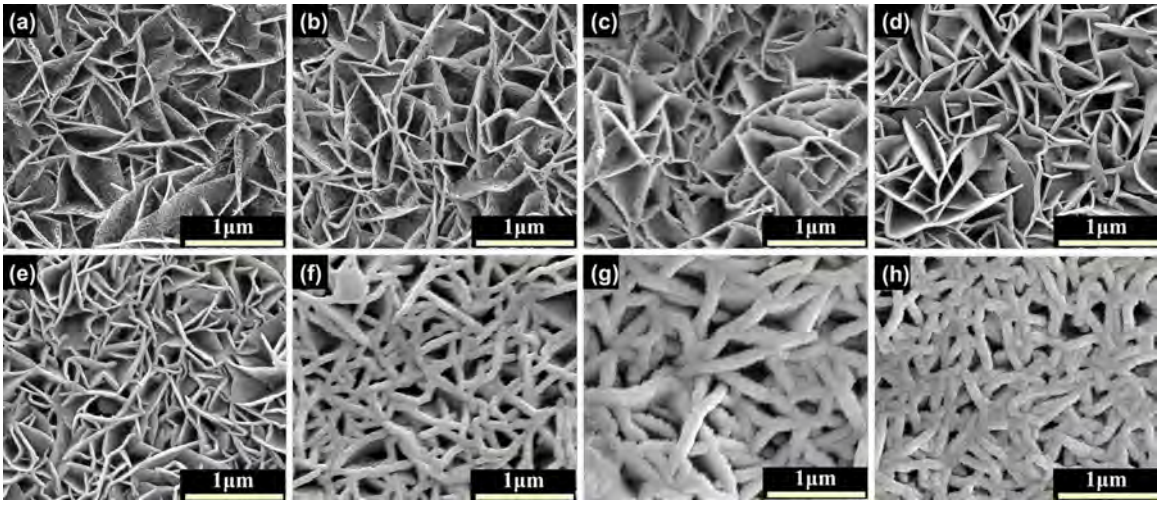

Fig. 3. The top-view SEM images of MnO_2/Au hybrid nanowall film. (a) Substrate-5; (b) Substrate-10; (c) Substrate-15; (d) Substrate-25; (e) Substrate-30; (f) Substrate-100; (g) Substrate-200; (h) Substrate-250.

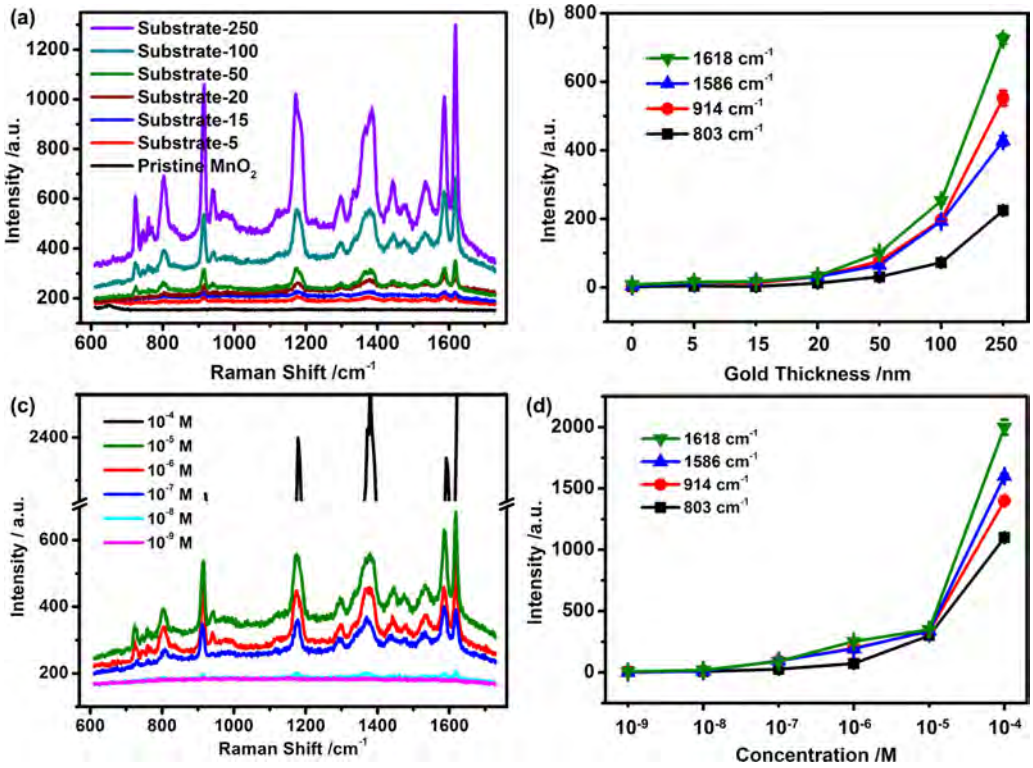

Fig. 4. (a) The raw Raman spectra of 1 μM CV on pristine MnO_2 nanowall, Substrate-5, Substrate-15, Substrate-20, Substrate-50, Substrate-100 and Substrate-250, respectively; (b) the Raman intensities of characteristic peaks with varied gold coating thickness; (c) the raw Raman spectra of different concentrations of CV (10^{-4} M, 10^{-5} M, 10^{-6} M, 10^{-7} M, 10^{-8} M, 10^{-9} M) on Substrate-100; (d) the Raman intensities of characteristic peaks with varied CV concentration.

nanoislands attached appears. Meanwhile, the space between adjacent nanowalls decreases as the thickness of gold film increasing (Fig. 3(a)–(h)).

SERS activity of the substrates was examined using CV as the Raman reporter. CV is the triarylmethane dye molecule widely used in biotechnological applications such as fluorescence imaging. It is frequently used to mimic biomolecules for testing the SERS effect on the substrates due to its distinct Raman features and well absorbability onto metal nanoparticles. To study the dependence of SERS signal on gold coating thickness, Raman measurements were conducted on the different SERS substrates with various thickness of gold layer. Fig. 4(a) shows the Raman spectra of CV using a series of SERS substrates. It can be seen that there is no CV characteristic peak observed on the pristine MnO_2 nanowall film. As for Substrate-5, weak Raman peaks of CV appear. As the nominal thickness of gold film increases, the intensity of all the characteristic peaks becomes stronger and stronger. The spectral feature characteristic peaks of CV are at about 803, 914, 1177, 1375, 1477, 1586 and 1618 cm^{-1}, which are assigned to ring C—H bend, ring skeletal vibration, N—Ph stretching and ring C—C stretching vibrations, respectively [34]. In particular, the peaks at 803 cm^{-1}, 914 cm^{-1}, 1586 cm^{-1} and 1618 cm^{-1} are selected as the reference peaks to monitor the intensity variation. Fig. 4(b) shows the tendency of intensity with the thickening of gold layer. Clearly, the intensities of all peaks exhibit the same rapid growth trend with the increasing of gold film. Fig. 4(c) displays the Raman spectra of CV with different concentrations on the Substrate-100. The intensities of the peaks at 803 cm^{-1}, 914 cm^{-1}, 1586 cm^{-1} and 1618 cm^{-1} are plotted as a function of the concentration of CV as shown in Fig. 4(d). Obviously, the intensities of the peaks grow rapidly with the increase of concentration of CV. The distinct peaks of CV can be detected even the concentration of CV down to 10^{-8} M, indicating a high sensitivity of the substrates.

The experimental EFs are estimated by the widely-accepted analytical EF approach and the equation given by [35]

$$EF = \frac{I_{SERS}}{C_{SERS}} \times \frac{C_{NR}}{I_{NR}}$$

where C_{SERS} and C_{NR} are the concentration of molecules used for SERS and normal Raman scattering measurements, respectively. I_{SERS} and I_{NR} are the integral intensity obtained by SERS and normal Raman scattering measurements, respectively. The fitting intensity of the ring C—C stretching band (1618 cm^{-1}) was chosen for EF calculation in this work. The C_{NR}/I_{NR} of about 7.56×10^{-2} is obtained by Raman measurement of CV saturated solution (2.2×10^{-1} M), which is very close to the reported value of 6.6×10^{-2} [36]. The maximum EF obtained from single spectrum in Fig. 4(c) can reach 2.31×10^{8} with concentration of 10^{-8} M, demonstrating a common signature of single molecule detection [5,6,37]. There are mainly two mechanisms which are believed to be important in the enhancement of the Raman signal: one is the surface plasmon resonance, known as electromagnetic enhancement; the other is the charge transfer resonances due to the formation of the complex between the adsorbate and metal structure, which is termed as chemical enhancement. In our case, both mechanisms are expected to enhance Raman signals. For the better understanding of the significant enhancement of MnO_2/Au substrate, FDTD simulations have been carried out using a structure model shown in Fig. 5(a). The diameter of gold nanoislands is configured as 20 nm and the thickness of nanowall 40 nm in our model in terms of the both SEM and TEM (Figure S2) observations. The local electromagnetic fields were calculated using commercial FDTD numerical simulation software (XFDTD, Remcom Inc.), which has recently been demonstrated to be highly useful in the study of the electromagnetic properties of metallic nanostructures for almost arbitrary geometry [38,39]. A planar wave with a wavelength of 532 nm

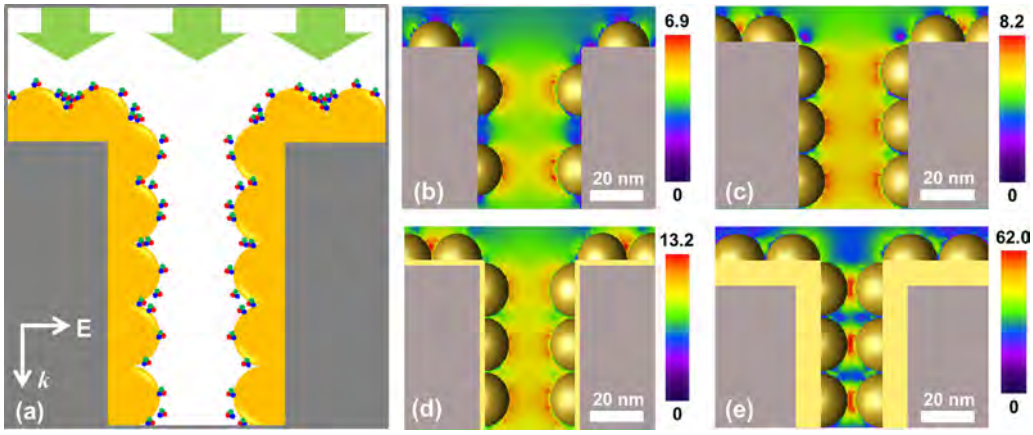

Fig. 5. The FDTD simulations for MnO_2/Au hybrid nanowall film; (a) the model of MnO_2/Au hybrid nanowall film for simulation; (b)–(e) FDTD simulations of the electric field distribution in cross-section view of MnO_2/Au hybrid nanowall film with varied gold thickness.

propagating along the ***k*** direction was input into the nanostructure with its polarization direction perpendicular to ***k***. The distributions of electric field intensity of different substrates are presented in Fig. 5(b)–(e) in cross-section view. Initially, the "hot spots" are located at the space surrounding the particles (Fig. 5(b)). As the deposition time grows, the gold nanoparticles connect to each other forming nanoisland, and then a gold film decorated with gold nanoislands comes into being. At the same time, the gap between two nanoislands is smaller. The enhancement field concentrated on the gap between two nanoislands as shown in Fig. 5(c). Prolonging the deposition time, the increased thickness of gold film lead to the narrow gap between the nanowalls, and a new "hot spots" area appears with superior enhancement which can be observed in Fig. 5(d) and (e). According to the simulations, the significant enhancement of Raman signal with increased gold coating in MnO_2/Au hybrid nanowall system can be mainly ascribed to the couplings of two gaps, i.e., one gap between the nanoislands and another gap between the nanowalls. At the beginning, the gap between nanoislands play a dominant role in the contribution of the enhancement; due to the change in structure with prolonging the deposition time, the coupling enhancement for the gap between two nanowalls play a leading role instead of that between two gold nanoislands. The enhancement of Raman signal can be simply defined as $\left|E/E_0\right|^4$ (E_0 is the incident field, and $E_0 = 1$ V/m) [40], where the local electric field for our model is calculated at a maximum of ca. 62.0 V/m, the EF originated from the coupling of the gaps can reach 10^7. This value is slightly smaller than that of experimental value, indicating that the chemical enhancement may also contribute to the total enhancement. As for the chemical enhancement, if the Fermi level of metal substrate can match with the highest occupied molecule orbital (HOMO) and the lowest occupied molecule orbital (LOMO) of the molecule symmetrically, the charge transfer will occur from metal to molecule easily or vice versa [41–43]. The Fermi level of Au is −5.1 eV relative to vacuum level, and the HOMO and LOMO of CV are −4.1 eV and −6.0 eV, respectively. Therefore, the charge transfer from CV to gold can take place in this system and is responsible for the additional enhancement of the Raman signal.

To verify the stability of this substrate, the Raman spectrum of Substrate-50 with 1 μM CV is measured one time per month over a period of 6 months. Fig. 6(a) shows the Raman spectra of the sample at different time. The variations of the intensities of characteristic peaks are shown in Fig. 6(b). It is evident that the Raman signals are not decreased significantly after six months, which indicates that the excellent stability of the obtained substrate. Since the laser exposure may lead to the damage of structure and poor stability, the Raman measurements have been repeatedly conducted on a same point of the Substrate-250 with 1 μM CV for 10 min under continuous laser exposure. Fig. 6(c) shows the Raman spectra collected on a single point of the substrate at different time. The intensities of characteristic peaks maintain during the entire procedure and no obvious reduction is observed (Fig. 6(d)), indicating that the laser effect on the Raman enhancement is negligible and allow us to carry out long-time Raman mapping measurements. The results prove that the as-developed MnO_2/Au hybrid nanowall films are robust SERS substrate with good stability under 6months storage and 10 min laser exposure (68.47 W/mm^2).

Another key issue of SERS substrate is the reproducibility of the enhancement, which is crucial in practical applications [44]. To verify the reproducibility of the enhancement, we performed large-area Raman mapping measurements on these substrates. Instead of the traditional random choice of measurement points, the Raman mapping technique can provide a reliable and convinced examination of overall surface enhancement of the SERS substrate by recording thousands of SERS spectra from a selected area. Fig. 7(a) shows a representative Raman map ($10 \times 10\ \mu m^2$, 50×50 pixels) of Substrate-200 with 1 μM CV, while the intensity of the ring C—C stretching (1618 cm^{-1}) vibrational peak is selected as the reference and 10 s acquisition time was adopted. The average intensity of all spectra in the mapping is 1827 arb.units, and the average EF can be calculated to be about 1.38×10^8. We further introduced roughness average (SA) to assess the reproducibility. The size of the pixel array, stored in the image data object, is defined as M × N, and then the number of pixels can be given by

$$< MN >= Number\ of\ Pixels = \sum_{j=1}^{N}\sum_{i=1}^{M} 1$$

The SA can be calculated from the intensity of each pixel in the image $z = (x_i, y_j)$. Naturally, the roughness average, SA, can be defined as

$$SA = \frac{1}{< MN >}\sum_{j=1}^{N}\sum_{i=1}^{M}\left|Z(x_i, y_j) - \bar{z}\right|$$

where $\bar{Z}$ representing the mean intensity

$$\bar{z} = \frac{1}{< MN >}\sum_{j=1}^{N}\sum_{i=1}^{M} Z(x_i, y_j)$$

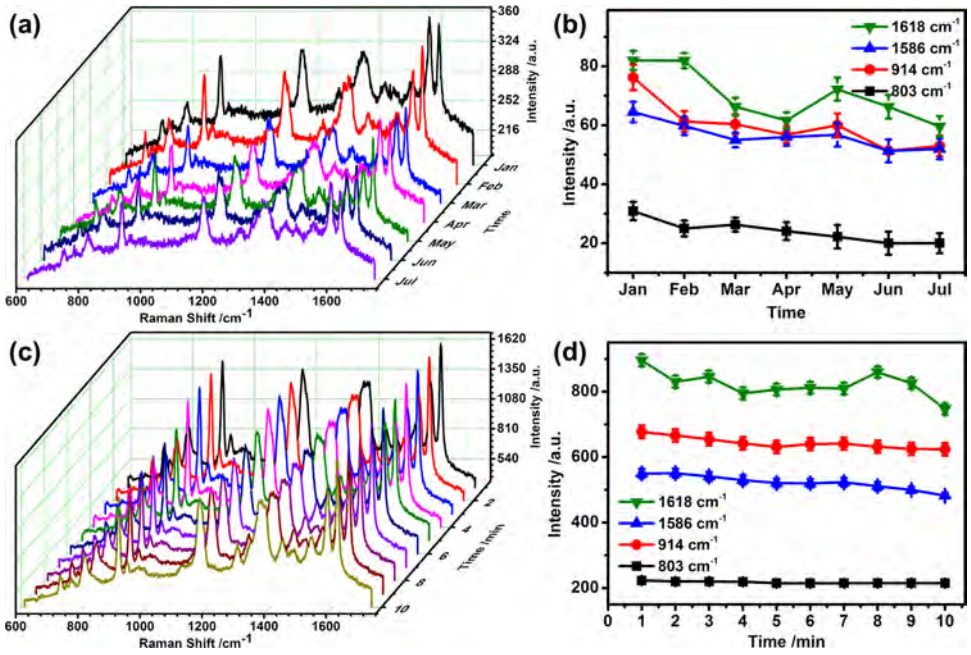

Fig. 6. (a) The raw Raman spectra of 1 μM CV on Substrate-50 collected at different time; (b) the variation of Raman intensity at different time; (c) the raw Raman spectra of 1 μM CV on Substrate-250 collected under 215 μW laser exposure; (d) the variation of Raman intensity at different time under 215 μW laser exposure.

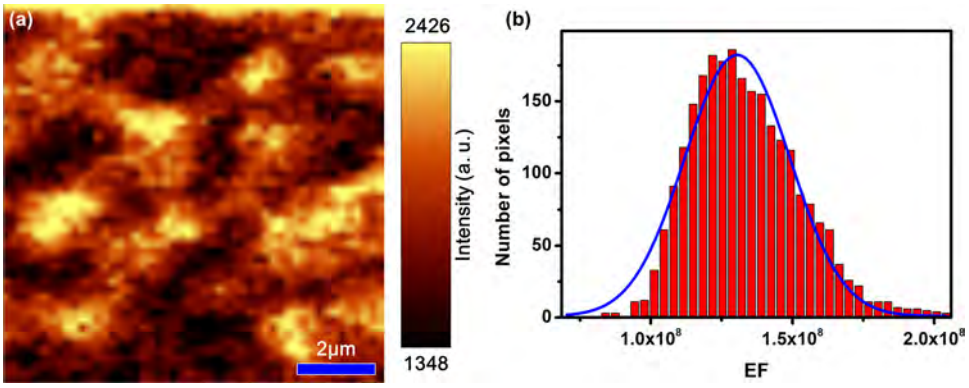

Fig. 7. (a) The Raman mapping of 1 μM CV on Substrate-200; (b) the histogram of EF distribution in mapping area.

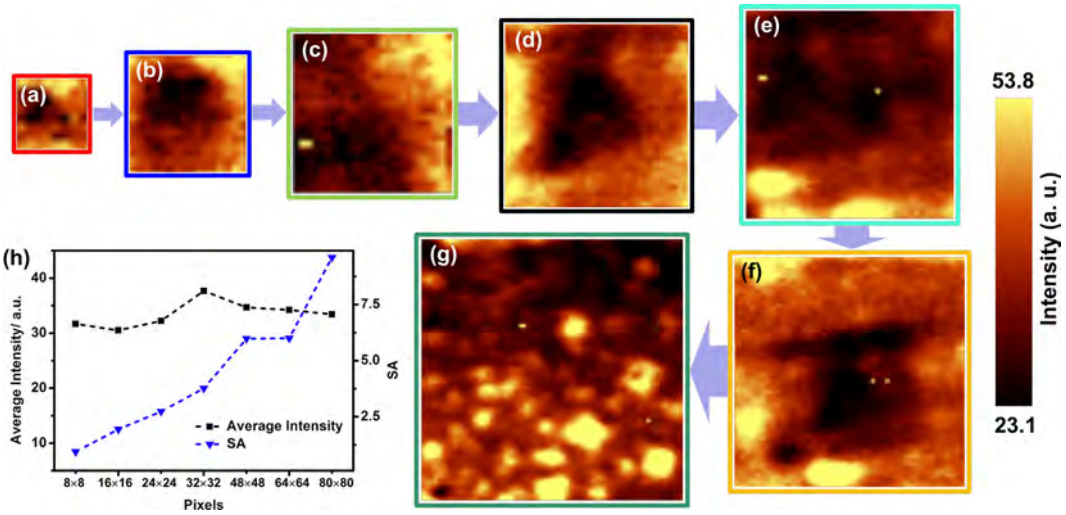

Fig. 8. The Raman mappings of 10 μM CV on Substrate-250 with varied area and pixels. (a) 8 × 8 pixels (3.5 × 3.5 μm^2); (b) 16 × 16 pixels (7.5 × 7.5 μm^2); (c) 24 × 24 pixels (11.5 × 11.5 μm^2); (d) 32 × 32 pixels (15.5 × 15.5 μm^2); (e) 48 × 48 pixels (23.5 × 23.5 μm^2); (f) 64 × 64 pixels (31.5 × 31.5 μm^2); (g) 80 × 80 pixels (39.5 × 39.5 μm^2); (h) the average intensity and SA as a function of mapping area.

The calculated SA of Fig. 7(a) is 2.72 arb.units. Fig. 7(b) shows the distribution of the EF and the blue curve is the fitting result with Gaussian. Obviously, the vast majority of EF values were concentrated on the average value. To further investigate the influence of scan area to the reproducibility, a series of mapping was performed with varied area on Substrate-250 with 10 μM CV. All the images have the same scanning step size of 500 nm and acquisition time of 1 s. Fig. 8(a)–(g) contains 8 × 8 pixels (3.5 × 3.5 μm^2), 16 × 16 pixels (7.5 × 7.5 μm^2), 24 × 24 pixels (11.5 × 11.5 μm^2), 32 × 32 pixels (15.5 × 15.5 μm^2), 48 × 48 pixels (23.5 × 23.5 μm^2), 64 × 64 pixels (31.5 × 31.5 μm^2) and 80 × 80 pixels (39.5 × 39.5 μm^2), respectively. Fig. 8(h) shows the variation of average intensity and SA with different mapping areas. As can be seen in Fig. 8(h), the SA values increase with the increasing mapping area. However, the average intensities of different mapping areas are almost the same. As a result, with the increase of the substrate area, the larger SA will reduce the reliability of single spectrum in random sampling case, but the average intensity obtained from Raman mapping maintains good reproducibility. Therefore, we believe that the results from Raman mapping can achieve better reproducibility than single spectrum measurement, and it is also more applicable to evaluate the performance of large-area SERS substrate.

4. Conclusion

In summary, we have developed a novel MnO_2/Au hybrid nanowall film substrates with simple and cheap hydrothermal route combined with vacuum thermal evaporation process. The detection sensitivity of the substrate can reach 10^{-8} M with Substrate-100, and 8 orders of magnitude enhancement factor can be achieved. The superior enhancement of as-developed SERS substrate can be ascribed to the LSPR in the gaps between two adjacent nanoislands and two adjacent nanowalls. The substrate shows excellent stability as there is negligible reduction in Raman intensity after 6 months storage and 10 min laser exposure (68.47 W/mm^2). The reproducibility of the substrate is also evaluated with average intensity and SA deduced from large-area Raman mapping. The average intensity almost maintains a constant for the different mapping areas, while SA value grows monotonously with the increasing mapping areas, which suggests that Raman mapping could provide more reliable and reproducible results as compared to single spectrum measurement. All the above-mentioned features combined with Raman mapping technique make MnO_2/Au nanowall film substrate quite promising to exploit SERS and related effects for routine Raman analyses.

Supplementary material

Detail of the EDS and TEM of MnO_2/Au hybrid nanowall film.

Acknowledgements

This work was financially supported by the National Natural Science Foundation of China (Grant No. 21376192), the Research Fund for the Doctoral Program of Higher Education China (Grant No. 20126101110017). The authors thank the Graphene Research and Characterization Center (GRCC) in Taizhou (Jiangsu Province, China) for the Raman measurements.

Appendix A. Supplementary data

Supplementary data associated with this article can be found, in the online version, at http://dx.doi.org/10.1016/j.apsusc.2015.02.014.

References

[1] M. Fleischmann, P.J. Hendra, A.J. McQuillan, Raman spectra of pyridine adsorbed at a silver electrode, Chem. Phys. Lett. 26 (1974) 163–166.
[2] L.A. Nafie, Recent advances in linear and nonlinear Raman spectroscopy. Part VII, J. Raman Spectrosc. 44 (2013) 1629–1648.
[3] X. Qian, X.H. Peng, D.O. Ansari, Q. Yin-Goen, G.Z. Chen, D.M. Shin, L. Yang, A.N. Young, M.D. Wang, S. Nie, In vivo tumor targeting and spectroscopic detection with surface-enhanced Raman nanoparticle tags, Nat. Biotechnol. 26 (2008) 83–90.
[4] K.V. Kong, Z. Lam, W.D. Goh, W.K. Leong, M. Olivo, Metal carbonyl-gold nanoparticle conjugates for live-cell SERS imaging, Angew. Chem. Int. Ed. 124 (2012) 9934–9937.
[5] S. Nie, S.R. Emory, Probing single molecules and single nanoparticles by surface-enhanced Raman scattering, Science 275 (1997) 1102–1106.
[6] K. Kneipp, Y. Wang, H. Kneipp, L.T. Perelman, I. Itzkan, R. Dasari, M.S. Feld, Single molecule detection using surface-enhanced Raman scattering (SERS), Phys. Rev. Lett. 78 (1997) 1667–1670.
[7] H. Liang, Z. Li, W. Wang, Y. Wu, H. Xu, Highly surface-roughened flower-like silver nanoparticles for extremely sensitive substrates of surface-enhanced Raman scattering, Adv. Mater. 21 (2009) 4614–4618.
[8] X. Li, G. Chen, L. Yang, Z. Jin, J. Liu, Multifunctional Au-coated TiO_2 nanotube arrays as recyclable SERS substrates for multifold organic pollutants detection, Adv. Funct. Mater. 20 (2010) 2815–2824.
[9] Z. Liu, L. Cheng, L. Zhang, C. Jing, X. Shi, Z. Yang, Y. Long, J. Fang, Large-area fabrication of highly reproducible surface enhanced Raman substrate via a facile double sided tape-assisted transfer approach using hollow Au-Ag alloy nanourchins, Nanoscale 6 (2014) 2567–2572.
[10] Z. Zhang, P. Yang, H. Xu, H. Zheng, Surface enhanced fluorescence and Raman scattering by gold nanoparticle dimers and trimmers, J. Appl. Phys. 113 (2013) 033102.
[11] D. Xu, J. Gu, W. Wang, X. Yu, K. Xi, X. Jia, Development of chitosan-coated gold nanoflowers as SERS-active probes, Nanotechnology 21 (2010) 375101.
[12] S. Shanmukh, L. Jones, J. Driskell, Y. Zhao, R. Dluhy, R.A. Tripp, Rapid and sensitive detection of respiratory virus molecular signatures using a silver nanorod array SERS substrate, Nano Lett. 6 (2006) 2630–2636.
[13] T. Qiu, Y. Zhou, J. Li, W. Zhang, X. Lang, T. Cui, P.K. Chu, Hot spots in highly Raman-enhancing silver nano-dendrites, J. Phys. D. Appl. Phys. 42 (2009) 175403.
[14] K. Sivashanmugan, J.D. Liao, J.W. You, C.L. Wu, Focused-ion-beam-fabricated Au/Ag multilayered nanorod array as SERS-active substrate for virus strain detection, Sensor. Actuator B. Chem. 181 (2013) 361–367.
[15] K. Liu, D. Li, R. Li, Q. Wang, S. Pan, W. Peng, M. Chen, Silver-decorated ZnO hexagonal nanoplate arrays as SERS-active substrates: An experimental and simulation study, J. Mater. Res. 28 (2013) 3374–3383.
[16] C.Y. Liu, M.M. Dvoynenko, M.Y. Lai, T.H. Chan, Y.R. Lee, J.K. Wang, Y.L. Wang, Anomalously enhanced Raman scattering from longitudinal optical phonons on Ag-nanoparticle-covered GaN and ZnO, Appl. Phys. Lett. 96 (2010) 033109.
[17] G. Shan, S. Zheng, S. Chen, Y. Chen, Y. Liu, Multifunctional ZnO/Ag nanorod array as highly sensitive substrate for surface enhanced Raman detection, Colloid. Surf. B 94 (2012) 157–162.
[18] F. Li, Y. Yuan, J. Luo, Q. Qin, J. Wu, Z. Li, X. Huang, Synthesis and characterization of ZnO-Ag core-shell nanocomposites with uniform thin silver layers, Appl. Surf. Sci. 256 (2010) 6076–6082.
[19] W. Song, Y. Wang, H. Hu, B. Zhao, Fabrication of surface-enhanced Raman scattering-active ZnO/Ag composite microspheres, J. Raman Spectrosc. 38 (2007) 1320–1325.
[20] Z.Y. Jiang, X.X. Jiang, S. Su, X.P. Wei, S.T. Lee, Y. He, Silicon-based reproducible and active surface-enhanced Raman scattering substrates for sensitive, specific, and multiplex DNA detection, Appl. Phys. Lett. 100 (2012) 203104.
[21] B. Zhang, H. Wang, L. Lu, K. Ai, G. Zhang, X. Cheng, Large-area silver-coated silicon nanowire arrays for molecular sensing using surface-enhanced Raman spectroscopy, Adv. Funct. Mater. 18 (2008) 2348–2355.
[22] S. Chan, S. Kwon, T.W. Koo, L.P. Lee, A.A. Berlin, Surface-enhanced Raman scattering of small molecules from silver-coated silicon nanopores, Adv. Mater. 15 (2003) 1595–1598.
[23] L. Yang, X. Jiang, W. Ruan, J. Yang, B. Zhao, W. Xu, J.R. Lombardi, Charge-transfer-induced surface-enhanced Raman scattering on Ag- TiO_2 nanocomposites, J. Phys. Chem. C 113 (2009) 16226–16231.
[24] D. Li, L. Pan, S. Li, K. Liu, S. Wu, W. Peng, Controlled preparation of uniform TiO_2-catalyzed silver nanoparticle films for surface-enhanced Raman scattering, J. Phys. Chem. C 117 (2013) 6861–6871.
[25] S. Jana, S. Pande, A.K. Sinha, S. Sarkar, M. Pradhan, M. Basu, S. Saha, T. Pal, A green chemistry approach for the synthesis of flower-like Ag-doped MnO2 nanostructures probed by surface-enhanced Raman spectroscopy, J. Phys. Chem. C 113 (2009) 1386–1392.
[26] X.D. Lin, V. Uzayisenga, J.F. Li, P.P. Fang, D.Y. Wu, B. Ren, Z.Q. Tian, Synthesis of ultrathin and compact Au@ MnO_2 nanoparticles for shell-isolated nanoparticle-enhanced Raman spectroscopy (SHINERS), J. Raman Spectrosc. 43 (2012) 40–45.
[27] Z.Y. Bao, J. Dai, D.Y. Lei, Y. Wu, Maximizing surface-enhanced Raman scattering sensitivity of surfactant-free Ag-Fe_3O_4 nanocomposites through optimization of silver nanoparticle density and magnetic self-assembly, J. Appl. Phys. 114 (2013) 124305.
[28] C.S. Rout, A. Kumar, T.S. Fisher, Carbon nanowalls amplify the surface-enhanced Raman scattering from Ag nanoparticles, Nanotechnology 22 (2011) 395704.

[29] X.D. Zhao, H.M. Fan, X.Y. Liu, H. Pan, H.Y. Xu, Pattern-dependent tunable adhesion of superhydrophobic MnO_2 nanostructured film, Langmuir 27 (2011) 3224–3228.
[30] E.M. Hicks, X. Zhang, S. Zou, O. Lyandres, K.G. Spears, G.C. Schatz, R.P. Van Duyne, Plasmonic properties of film over nanowell surfaces fabricated by nanosphere lithography, J. Phys. Chem. B 109 (2005) 22351–22358.
[31] Q. Yu, P. Guan, D. Qin, G. Golden, P.M. Wallace, Inverted size-dependence of surface-enhanced Raman scattering on gold nanohole and nanodisk arrays, Nano Lett. 8 (2008) 1923–1928.
[32] F. De Angelis, F. Gentile, F. Mecarini, G. Das, M. Moretti, P. Candeloro, M.L. Coluccio, G. Cojoc, A. Accardo, C. Liberale, R.P. Zaccaria, G. Perozziello, L. Tirinato, A. Toma, G. Cuda, R. Cingolani, E. Di Fabrizio, Breaking the diffusion limit with super-hydrophobic delivery of molecules to plasmonic nanofocusing SERS structures, Nat. Photonics 5 (2011) 682–687.
[33] R. Alvarez-Puebla, B. Cui, J.P. Bravo-Vasquez, T. Veres, H. Fenniri, Nanoimprinted SERS-active substrates with tunable surface plasmon resonances, J. Phys. Chem. C 111 (2007) 6720–6723.
[34] A. Kudelski, Raman studies of rhodamine 6G and crystal violet sub-monolayers on electrochemically roughened silver substrates: Do dye molecules adsorb preferentially on highly SERS-active sites, Chem. Phys. Lett. 414 (2005) 271–275.
[35] E.C. Le Ru, E. Blackie, M. Meyer, P.G. Etchegoin, Surface enhanced Raman scattering enhancement factors: a comprehensive study, J. Phys. Chem. C 111 (2007) 13794–13803.
[36] I. Chakraborty, S. Bag, U. Landman, T. Pradeep, Atomically precise silver clusters as new SERS substrates, J. Phys. Chem. Lett. 4 (2013) 2769–2773.
[37] N.P. Pieczonka, R.F. Aroca, Single molecule analysis by surfaced-enhanced Raman scattering, Chem. Soc. Rev. 37 (2008) 946–954.
[38] Z.Y. Zhang, Y.J. Liu, Q. Zhao, Y.P. Zhao, The effect of layer absorbance for complex surface enhanced Raman scattering substrates, Appl. Phys. Lett. 94 (2009) 143107.
[39] Y. Zhao, Y. Qin, W. Cao, Z. Zhang, Enhancing the electric fields around the nanorods by using metal grooves, Sci. China Phys. Mech. 55 (2012) 1763–1768.
[40] M. Kerker, D.S. Wang, H. Chew, Surface enhanced Raman scattering (SERS) by molecules adsorbed at spherical particles, Appl. Opt. 19 (1980) 3373–3388.
[41] A. Campion, P. Kambhampati, Surface-enhanced Raman scattering, Chem. Soc. Rev. 27 (1998) 241–250.
[42] A. Otto, The 'chemical' (electronic) contribution to surface-enhanced Raman scattering, J. Raman Spectrosc. 36 (2005) 497–509.
[43] X. Ling, L. Xie, Y. Fang, H. Xu, H. Zhang, J. Kong, M.S. Dresselhaus, J. Zhang, Z. Liu, Can graphene be used as a substrate for Raman enhancement, Nano Lett. 10 (2009) 553–561.
[44] X.T. Wang, W.S. Shi, G.W. She, L.X. Mu, S.T. Lee, High-performance surface-enhanced Raman scattering sensors based on Ag nanoparticles-coated Si nanowire arrays for quantitative detection of pesticides, Appl. Phys. Lett. 96 (2010) 053104.